Model-based Stabilization of Vortex Shedding with CFD Verification

Milan Milovanovic, Marek Gayer, Joris Michielsen and Ole Morten Aamo

***Abstract*— We establish the link between backstepping controllers previously designed for the Ginzburg-Landau model of vortex shedding and the actual flow dynamics, represented by a Navier-Stokes solver, and demonstrate, for the first time in CFD simulations, the effectiveness of this class of controllers in attenuating vortex shedding.**

I. Introduction

In flows past submerged obstacles, the phenomenon of vortex shedding occurs provided the Reynolds number is sufficiently large. A popular model flow for studying vortex suppression by means of open-loop or feedback control, is the flow past a two-dimensional circular cylinder, as sketched in Fig. 1 where the the so-called von Kármán vortex street is visualized using passive tracer particles. For Reynolds numbers slightly larger than the critical value for onset of vortex shedding (which is approximately $\mathrm{Re}_c = 47$), several authors have successfully suppressed vortex shedding in numerical simulations using various simple feedback control configurations. In [1], a pair of suction/blowing slots positioned on the cylinder wall were used for actuation, and shedding was suppressed for $\mathrm{Re} = 60$, using proportional feedback from a single velocity measurement taken some distance downstream of the cylinder. For $\mathrm{Re} = 80$, vortex shedding was reduced, but not completely suppressed. In [2], the same actuation configuration was tried using feedback from a pair of pressure sensors located on the cylinder wall for $\mathrm{Re} = 60$. This attempt was unsuccessful, but by adding a third actuation slot shedding was reduced considerably, even at $\mathrm{Re} = 80$. Although some success in controlling vortex shedding has been achieved in numerical simulations, rigorous control designs are scarce due to the complexity of designing controllers based on the Navier-Stokes equation. A much simpler model, the Ginzburg-Landau (GL) equation with appropriate coefficients, has been found to model well the dynamics of vortex shedding near the critical value of the Reynolds number [3]. In [4], it was shown numerically that the GL model for Reynolds numbers close to Re_c can be stabilized using proportional feedback from a single measurement downstream of the cylinder, to local forcing at the location of the cylinder. Systematic control designs for finite dimensional approximations of the model from [4] were developed in [5], [6] for the linearized model, and in [7] for the nonlinear model. The designs were in principle valid for any Reynolds number. In [8] and [9], boundary control laws based on the non-discretized, linearized GL equation were rigorously derived for the state feedback and boundary output feedback cases, respectively. They were shown to effectively attenuate vortex shedding for the nominal case with GL as the system plant as well as the design model. The link between the GL-based controller and the physical system, represented by a Navier-Stokes (NS) solver, has not yet been established. Closing this gap is the main topic of this paper, which includes tailoring a CFD code for flow control simulations, fitting the GL model to CFD data, and designing the input-output links between the GL-based controller and the NS-based simulator. Putting all pieces together, we demonstrate in CFD simulations the successful stabilization of vortex shedding by means of the GL-based controller.

This work was supported by the BVV program at NTNU (Program on Computational Science and Visualization). The second author acknowledges support from the ERCIM exchange program.

M. Milovanovic, M. Gayer, and O.M. Aamo are with the Department of Engineering Cybernetics, NTNU. J. Michielsen is with TU Eindhoven.

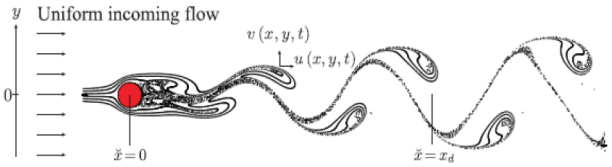

Fig. 1. Vortex shedding from a cylinder visualized by passive tracer particles

II. The Ginzburg-Landau Model

The dynamics of the cylinder wake is governed by the Navier-Stokes equation. In [4], however, a simplified model was suggested in terms of the Ginzburg-Landau equation

$$\begin{aligned}\frac{\partial A}{\partial t} &= a_1 \frac{\partial^2 A}{\partial \breve{x}^2} + a_2(\breve{x})\frac{\partial A}{\partial \breve{x}} + a_3(\breve{x})A \\ &\quad + a_4 |A|^2 A + \delta(\breve{x}-1)u, \end{aligned} \tag{1}$$

where A is a complex-valued function of one spatial variable, $\breve{x} \in \mathbb{R}$, and time, $t \in \mathbb{R}_+$. The boundary conditions are $A(\pm\infty, t) = 0$. The control input, denoted u, is in the form of point actuation at the location of the cylinder, and the coefficients a_i, $i = 1, .., 4$, were fitted to data from laboratory experiments in [4]. δ denotes the Dirac distribution. $A(\breve{x}, t)$ may represent any physical variable (velocities (u, v) or pressure p), or derivations thereof, along the centerline of the 2D cylinder flow. The choice will have an impact on the performance of the Ginzburg-Landau model, and associating A with the transverse fluctuating velocity $v(\breve{x}, \breve{y} = 0, t)$ seems to be a particularly good choice [10]. As pointed out in [6], the model is derived for Reynolds numbers close to the critical Reynolds number for onset of vortex shedding, but

has been shown to remain accurate far outside this vicinity for a wide variety of flows.

In [8], [9] a simplification of (1) was considered, obtained by linearizing around the zero solution, discarding the upstream subsystem by replacing the local forcing at $\breve{x} = 0$ with boundary input at this location, and truncating the downstream subsystem at some $x_d \in (0, -\infty)$. The truncation of the system was justified by noting that the upstream subsystem is approximately uniform flow, whereas the downstream subsystem can be approximated to any desired level of accuracy by selecting x_d sufficiently far from the cylinder.[1] The resulting system is given by

$$\frac{\partial A}{\partial t} = a_1 \frac{\partial^2 A}{\partial \breve{x}^2} + a_2(\breve{x}) \frac{\partial A}{\partial \breve{x}} + a_3(\breve{x}) A \tag{2}$$

for $\breve{x} \in (0, x_d)$, with boundary conditions

$$A(0,t) = u(t) \text{ and } A(x_d, t) = 0, \tag{3}$$

where $A : [0, x_d] \times \mathbb{R}_+ \to \mathbb{C}$, $a_2 \in C^2([0, x_d]; \mathbb{C})$, $a_3 \in C^1([0, x_d]; \mathbb{C})$, $a_1 \in \mathbb{C}$, and $u : \mathbb{R}_+ \to \mathbb{C}$ is the control input. a_1 is assumed to have strictly positive real part. In [8], stabilizing state feedback boundary control laws for system (2)–(3) were derived based on the backstepping methodology [11], [12], [13], [14]. The control laws made use of distributed measurements in a finite region downstream of the cylinder. In practice, the physical actuation could be for instance micro/synthetic jet actuators, distributed on the cylinder surface, and a possible choice for the physical sensing could be pressure sensors distributed on the cylinder surface.

III. State Feedback Control Design

The state feedback controller designed in [8] takes the form

$$\begin{aligned} u(t) &= \int_0^{x_d} \frac{1}{x_d}[k_1(\frac{x_d - \breve{x}}{x_d}) - ik_{c,1}(\frac{x_d - \breve{x}}{x_d})]A(\breve{x}, t) \\ &\quad \times \exp\left(\frac{1}{2a_1}\int_0^{\breve{x}} a_2(\tau)d\tau\right) d\breve{x} \end{aligned} \tag{4}$$

where i denotes the imaginary unit, and k_1 and $k_{c,1}$ are the controller kernels which can be computed as the solution of a certain hyperbolic partial differential equation. We repeat some details from [8] for clarity and completeness. It is convenient to rewrite the GL equation to obtain two coupled partial differential equations in real variables and coefficients by defining $\rho(x,t) = \Re(B(x,t)) = \left(B(x,t) + \bar{B}(x,t)\right)/2$, and $\iota(x,t) = \Im(B(x,t)) = \left(B(x,t) - \bar{B}(x,t)\right)/(2i)$, where $x = (x_d - \breve{x})/x_d$, $B(x,t) = A(\breve{x}, t)\exp\left(\frac{1}{2a_1}\int_0^{\breve{x}} a_2(\tau)\, d\tau\right)$, and $\bar{}$ denotes complex conjugation. Equation (2) becomes

$$\begin{aligned} \rho_t &= a_R \rho_{xx} + b_R(x)\rho - a_I \iota_{xx} - b_I(x)\iota, \\ \iota_t &= a_I \rho_{xx} + b_I(x)\rho + a_R \iota_{xx} + b_R(x)\iota, \end{aligned} \tag{5}$$

for $x \in (0,1)$, with boundary conditions

$$\begin{aligned} \rho(0,t) &= 0,\ \iota(0,t) = 0, \text{ and} \\ \rho(1,t) &= u_R(t),\ \iota(1,t) = u_I(t), \end{aligned} \tag{6}$$

where $a_R \triangleq \Re(a_1)/x_d^2$, $a_I \triangleq \Im(a_1)/x_d^2$, and

$$\begin{aligned} b_R(x) &\triangleq \Re\left(a_3(\breve{x}) - \tfrac{1}{2}a_2'(\breve{x}) - \tfrac{1}{4a_1}a_2^2(\breve{x})\right), \\ b_I(x) &\triangleq \Im\left(a_3(\breve{x}) - \tfrac{1}{2}a_2'(\breve{x}) - \tfrac{1}{4a_1}a_2^2(\breve{x})\right). \end{aligned} \tag{7}$$

The state feedback stabilization problem is solved by searching for a coordinate transformation in the form

$$\begin{aligned} \breve{\rho}(x,t) &= \rho(x,t) \\ &\quad - \int_0^x [k(x,y)\rho(y,t) + k_c(x,y)\iota(y,t)]\, dy, \end{aligned} \tag{8}$$

$$\begin{aligned} \breve{\iota}(x,t) &= \iota(x,t) \\ &\quad - \int_0^x [-k_c(x,y)\rho(y,t) + k(x,y)\iota(y,t)]\, dy, \end{aligned} \tag{9}$$

transforming system (5)–(6) into

$$\begin{aligned} \breve{\rho}_t &= a_R \breve{\rho}_{xx} + f_R(x)\breve{\rho} - a_I \breve{\iota}_{xx} - f_I(x)\breve{\iota}, \\ \breve{\iota}_t &= a_I \breve{\rho}_{xx} + f_I(x)\breve{\rho} + a_R \breve{\iota}_{xx} + f_R(x)\breve{\iota}, \end{aligned} \tag{10}$$

for $x \in (0,1)$, with boundary conditions

$$\breve{\rho}(0,t) = \breve{\iota}(0,t) = \breve{\rho}(1,t) = \breve{\iota}(1,t) = 0. \tag{11}$$

By the choice of f_R and f_I, system (10)–(11) can be given any desired level of stability. The corresponding stable behaviour for the original system is ensured by the control input

$$u_R(t) = \int_0^1 [k_1(y)\rho(y,t) + k_{c,1}(y)\iota(y,t)]\, dy, \tag{12}$$

$$u_I(t) = \int_0^1 [-k_{c,1}(y)\rho(y,t) + k_1(y)\iota(y,t)]\, dy, \tag{13}$$

where $k_1(y) = k(1,y)$, $k_{c,1}(y) = k_c(1,y)$. The skew-symmetric form of (12)–(13) is postulated from the skew-symmetric form of (5). The following result was proven in [8][2].

Theorem 1:

i. The pair of kernels, $k(x,y)$ and $k_c(x,y)$, satisfy the partial differential equation

$$\begin{aligned} k_{xx} &= k_{yy} + \beta(x,y)k + \beta_c(x,y)k_c, \\ k_{c,xx} &= k_{c,yy} - \beta_c(x,y)k + \beta(x,y)k_c, \end{aligned} \tag{14}$$

for $(x,y) \in \mathcal{T} = \{x, y : 0 < y < x < 1\}$, with boundary conditions

$$\begin{aligned} k(x,x) &= -\tfrac{1}{2}\textstyle\int_0^x \beta(\gamma,\gamma)d\gamma,\ k(x,0) = 0, \\ k_c(x,x) &= \tfrac{1}{2}\textstyle\int_0^x \beta_c(\gamma,\gamma)d\gamma,\ k_c(x,0) = 0, \end{aligned} \tag{15}$$

where

$$\beta(x,y) = \frac{a_R(b_R(y) - f_R(x)) + a_I(b_I(y) - f_I(x))}{a_R^2 + a_I^2}, \tag{16}$$

[1] This claim is postulated from the observation that the local damping effect in (1) increases with increasing distance from the cylinder, which follows from the coefficients reported in [4].

[2] In the statement of Theorem 1 and in the text in Section 8 of [8], $L_\infty(0,1)$ should be replaced by $H_3(0,1)$. Furthermore, the initial conditions must be compatible with the boundary conditions.

$$\beta_c(x,y) = \frac{a_R\left(b_I(y) - f_I(x)\right) - a_I\left(b_R(y) - f_R(x)\right)}{a_R^2 + a_I^2}. \tag{17}$$

The equation (14) with boundary conditions (15) has a unique $C^2(\mathcal{T})$ solution, given by

$$\begin{array}{rcl} k(x,y) & = & \sum_{n=0}^{\infty} G_n(x+y, x-y), \\ k_c(x,y) & = & \sum_{n=0}^{\infty} G_{c,n}(x+y, x-y), \end{array} \tag{18}$$

where

$$G_0(\xi,\eta) = -\frac{1}{4}\int_{\eta}^{\xi} b(\tau,0)\, d\tau, \tag{19}$$

$$G_{c,0}(\xi,\eta) = \frac{1}{4}\int_{\eta}^{\xi} b_c(\tau,0)\, d\tau, \tag{20}$$

$$\begin{aligned} G_{n+1}(\xi,\eta) = {} & \frac{1}{4}\int_{\eta}^{\xi}\int_{0}^{\eta} b(\tau,s)\, G_n(\tau,s)\, ds d\tau \\ & + \frac{1}{4}\int_{\eta}^{\xi}\int_{0}^{\eta} b_c(\tau,s)\, G_{c,n}(\tau,s)\, ds d\tau, \end{aligned} \tag{21}$$

$$\begin{aligned} G_{c,n+1}(\xi,\eta) = {} & -\frac{1}{4}\int_{\eta}^{\xi}\int_{0}^{\eta} b_c(\tau,s)\, G_n(\tau,s)\, ds d\tau \\ & + \frac{1}{4}\int_{\eta}^{\xi}\int_{0}^{\eta} b(\tau,s)\, G_{c,n}(\tau,s)\, ds d\tau, \end{aligned} \tag{22}$$

and

$$b(\xi,\eta) = \beta\left(\frac{\xi+\eta}{2}, \frac{\xi-\eta}{2}\right), \tag{23}$$

$$b_c(\xi,\eta) = \beta_c\left(\frac{\xi+\eta}{2}, \frac{\xi-\eta}{2}\right). \tag{24}$$

ii. The inverse of (8)–(9) exists and is in the form

$$\begin{aligned} \rho(x,t) = {} & \breve{\rho}(x,t) \\ & - \int_0^x \left[l(x,y)\,\breve{\rho}(y,t) + l_c(x,y)\,\breve{\iota}(y,t)\right] dy, \end{aligned} \tag{25}$$

$$\begin{aligned} \iota(x,t) = {} & \breve{\iota}(x,t) \\ & - \int_0^x \left[-l_c(x,y)\,\breve{\rho}(y,t) + l(x,y)\,\breve{\iota}(y,t)\right] dy, \end{aligned} \tag{26}$$

where l and l_c are $C^2(\mathcal{T})$ functions. l and l_c can be expressed similarly to k and k_c in (18)–(22), but we omit their explicit definition due to page limitations.

iii. Suppose $c > 0$, and select f_R and f_I such that

$$\sup_{x\in[0,1]}\left(f_R(x) + \frac{1}{2}\left|f_I'(x)\right|\right) \leq -c. \tag{27}$$

Then for any initial data $(\rho_0, \iota_0) \in H_3(0,1)$, compatible with the boundary conditions, the system (5)–(6) in closed loop with the control law (12)–(13) has a unique classical solution $(\rho,\iota) \in C^{2,1}((0,1)\times(0,\infty))$ and is exponentially stable at the origin in the $L_2(0,1)$ and $H_1(0,1)$ norms.

In [8], it was shown that a particular choice of f_R and f_I, that depend on x_d in a specific way, results in state feedback kernel functions that are invariant of x_d and vanish in $[x_s, x_d]$, where x_s is a constant that can be deduced from the coefficients of (2). This implies that if the domain is truncated at some $x_s \leq x_d$ for the purpose of computing the feedback kernel functions, the resulting state feedback will stabilize the plant evolving on the semi-infinite domain $(0,\infty)$. This is achieved by avoiding the complete cancellation of the terms involving b_R and b_I in (5) by using a target system (10) that contains the natural damping that exists in the plant downstream of x_s. It ensures that only cancellation/domination of the source of instability is performed in the design, and is similar to common practice in design of finite dimensional backstepping controllers, where one seeks to leave unaltered terms that add to the stability while cancelling terms that don't. The result is less complexity, and better robustness properties. An interesting property of our design is that it requires the solution of a linear hyperbolic PDE, which is an advantage when compared to other methods, such as LQG requiring the solution of a Riccati equation, which is quadratic. In fact, for a plant much simpler than the linearized Ginzburg-Landau model, solving the hyperbolic PDE is reported in [11] to take an order of magnitude less computational time than solving the Riccati equation. Although the series (18) happen to converge rapidly, they can be computed by a more efficient numerical scheme that was developed in [11]. Further details can be found in [8].

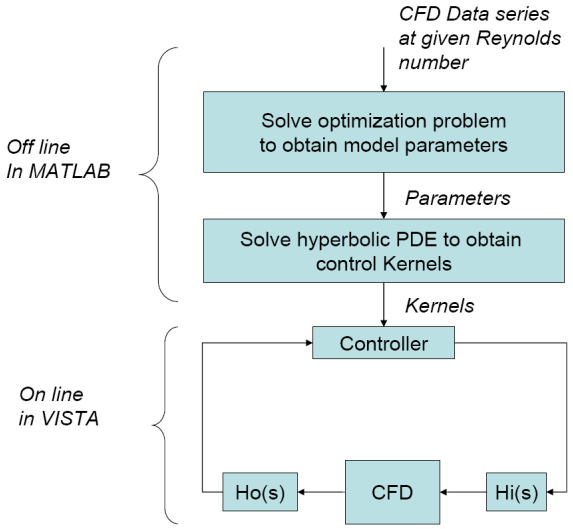

Fig. 2. Simulation setup.

IV. Simulation Setup

The simulation setup is shown schematically in Fig. 2. It contains offline computations performed in MATLAB that produce GL parameters for a given Reynolds number and the corresponding controller kernels. The online computations, or the closed-loop simulations, are performed with the CFD code VISTA. We next present details of the simulation setup.

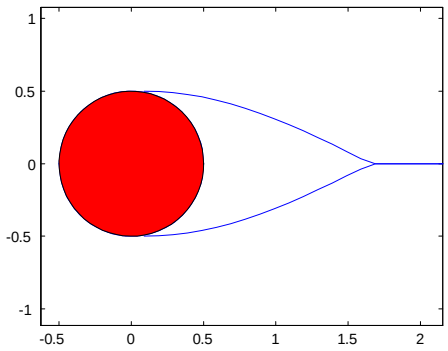

Fig. 3. Curves along which transverse velocity is measured.

A. GL/CFD Connection

While A in principle may represent any physical variable in the flow, the transverse fluctuation velocity along the flow centerline is a particularly good choice. For the interior flow, we define two curves originating at the actuation slots and converging at the flow centerline as they stretch into the 2D flow domain (see Fig. 3). Transverse velocity is measured along these curves, denoted $v_l(\breve{x},t)$ and $v_u(\breve{x},t)$ in Fig. 3, and related to A as

$$Re(A) := v(\breve{x},t) = \frac{1}{2}\left(v_l(\breve{x},t) + v_u\breve{x},t)\right). \qquad (28)$$

The imaginary part of A is reconstructed based on modes of the GL equation having the form

$$A(\breve{x},t) = \Phi(\breve{x})exp(i\kappa\breve{x} - i\omega t). \qquad (29)$$

We approximate $Im(A)$ by shifting $Re(A)$ in space corresponding roughly to $\Delta\breve{x} = TU/4$, where T is the shedding period and U is the streamwise velocity. Having obtained A as described, the control input is computed using Equation (4). With the real part of A representing transverse velocity, the control actuation which is a Dirichlet boundary condition at the actuation end in the GL model, can be realized in the CFD code by jets on the cylinder surface. We do this by employing two slots configured as shown in Fig. 4, close to the separation layers for effectiveness [15]. When one slot applies suction the other applies an equal amount of blowing, thereby maintaining the mass balance in the system. The actuation is thus suction and blowing whose size is given by the real part of u computed from Equation (4).

B. Obtaining GL parameters

To estimate the parameters for the Ginzburg-Landau equation, an iterative search is carried out where the difference between the model solution and a data set is minimized. The data set is extracted from CFD simulations, where the transition between laminar flow and fully developed vortex shedding is made by changing the Reynolds number from subcritical ($R_e = 40$) to supercritical ($R_e = 60$). The transverse velocity component, $v(\breve{x},t)$, is measured as described in the previous section along the curves shown in

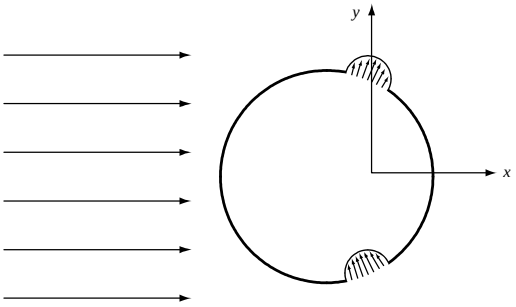

Fig. 4. Suction/blowing actuation slots.

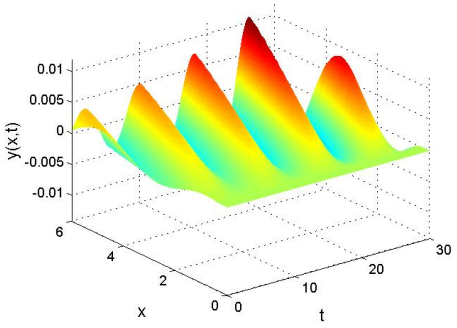

Fig. 5. CFD data set.

Fig. 3. The resulting data set is shown in Fig. 5, where the transition into vortex shedding is clearly visible.

By studying CFD data and simulations of the GL equation (3), some apriori assumptions were made for the parameters a_1, $a_2(\breve{x})$ and $a_3(\breve{x})$ before posing the optimization problem. The diffusion contribution is assumed to be constant, $a_1 = 1/R_e$, because it corresponds to the dynamic viscosity of the fluid. $a_2(\breve{x})$ is assumed to be real-valued, while $a_3(\breve{x}) = a_{3R}(\breve{x}) + ia_{3I}(\breve{x})$ is complex-valued with components $a_{3R}(\breve{x})$ and $a_{3I}(\breve{x})$ real-valued. The functions $a_2(\breve{x})$, $a_{3R}(\breve{x})$ and $a_{3I}(\breve{x})$ are approximated as polynomials in the optimization problem.

To obtain an accurate estimate for the parameters, a

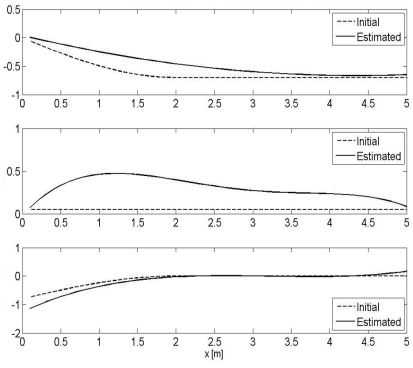

Fig. 6. Estiamated parameters a_2, a_{3R}, a_{3I} ordered from top to bottom

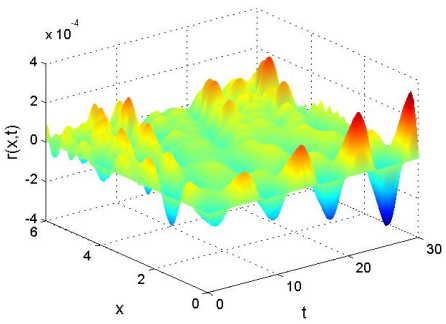

Fig. 7. The residue between real CFD data and GL simulations.

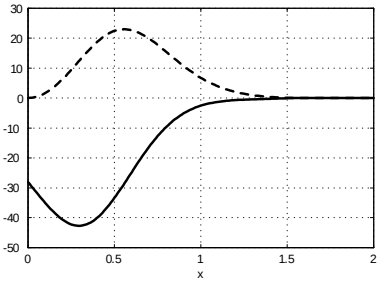

Fig. 8. Controller kernels, k_1 (solid line) and $k_{c,1}$ (dashed line).

finite difference scheme for the GL equation is derived based on the knowledge that the system is dominated by advection. To avoid numerical diffusion, which leads to severe damping in the advection term, the Lax-Wendroff scheme is used. This scheme is second order accurate in space and time. To keep this accuracy a central difference scheme for the spatial second order derivative in the diffusion term is combined with the Crank-Nicholson scheme as time integration method for both the diffusion and advection terms. Denoting the solution of the difference scheme on the spatial grid $\{x_1, x_2, ..., x_m\}$ as $A_R = [A_R(x_1) \ ... \ A_R(x_m)]^T$ and $A_I = [A_I(x_1) \ ... \ A_I(x_m)]^T$ (corresponding to the real and imaginary parts), the optimization method is based on the least squares formulation

$$c^* = \arg\min_c f(c) = \arg\min_c \frac{1}{N} \sum_{n=1}^{N} \frac{1}{2} r^n(c)^T r^n(c)$$

where $r^n(c) = A_R^n(c) - v^n$ and n specifies the discrete time step, c is a vector with unknown parameters to be determined, and v^n is the CFD data at time step n. This unconstrained nonlinear optimization problem is solved with the Levenberg-Marquardt method.

For the data set shown in Fig. 5, the initial parameter guess and the converged parameters are presented in Fig. 6. The error when comparing the data set with simulations with the GL equation using these paramters is shown in Fig. 7. The parameters are effetively estimated.

With parameters of the Ginzburg-Landau equation in hand, the controller kernels, $k_1(\breve{x})$ and $k_{c,1}(\breve{x})$, are computed from (18)–(24). They are shown in Fig. 8.

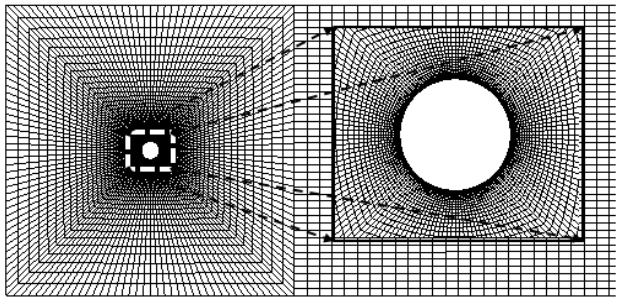

Fig. 9. Computational grid with zoom around cylinder.

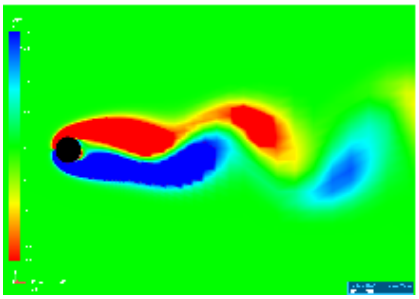

Fig. 10. Vorticity map at $t = 0$. Fully developed vortex shedding.

C. CFD system

As a basis for our CFD simulations we use VISTA, which is a general purpose CFD code developed by SINTEF Applied Mathematics. At the core of VISTA is a Navier-Stokes solver written in C++ using the Diffpack library for finite element modelling. We have tailored VISTA by adding C++ objects that realize actuation and sensing devices, as well as controller computations. This module takes as input the controller kernels that are computed offline in MATLAB. General purpose grid generators can be used to produce computational grids for VISTA. Fig. 9 shows the grid used in our simulations, which was verified in [16] to be sufficiently fine for the Reynolds numbers that we use in this paper.

V. Simulation Results

The intial condition for our simulation is fully developed vortex shedding at $R_e = 60$. Fig. 10 shows a vorticity map of the flow at $t = 0$. The von Kármán vortex street is clearly visible. Vortex shedding subjects the bluff body, in this case the cylinder, to periodic forcing, and would in any physical system induce potentially destructive vibrations. The transverse force is shown in Fig. 11, for our controlled simulation. The controller effectively attenuates the forcing. Fig. 12 shows the input to our controller, $\mathrm{Re}(A)$, as a function of time, while Fig. 13 and Fig. 14 show vorticity maps at $t = 20s$ and $t = 100s$. Clearly, vortex shedding is completely removed in Fig. 14. The control actuation that achieves this is shown in Fig. 15.

VI. Conclusion

In this paper, we have established the link between controllers previously designed for the Ginzburg-Landau

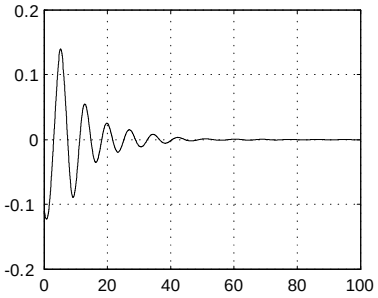

Fig. 11. Lift coefficient.

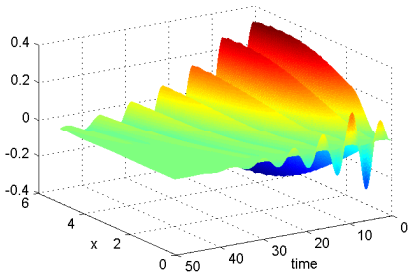

Fig. 12. Input to the controller, $A(\check{x}, t)$.

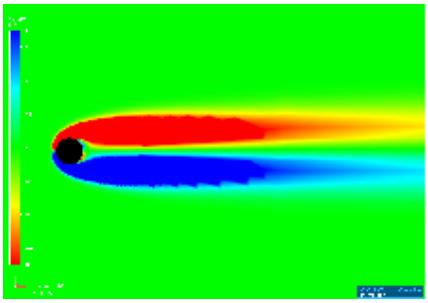

Fig. 14. Vorticity map at $t = 100$. Completely stabilized flow.

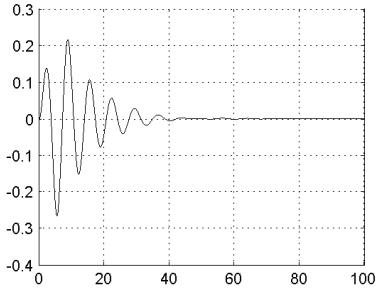

Fig. 15. The control input.

model of vortex shedding and the actual flow dynamics. The latter has been represented by a CFD package that solves the Navier-Stokes system for the 2D cylinder flow. Vortex shedding is successfully removed by the control at Reynolds number $R_e = 60$. The control design is systematic and can potentially be repeated for higher Reynolds numbers, although it is likely to be limited by the validity of the Ginzburg-Landau model at high Reynolds number. Ongoing work is focused at exploring this issue, while future work will involve CFD verification of the output feedback problem, which was solved for the GL equation in [9].

REFERENCES

[1] D. Park, D. Ladd, and E. Hendricks, "Feedback control of von kármán vortex shedding behind a circular cylinder at low reynoylds numbers," *Physics of fluids*, vol. 7, no. 7, pp. 2390–2405, 1994.

[2] M. Gunzburger and H. Lee, "Feedback control of karman vortex shedding," *Transactions of the ASME*, vol. 63, pp. 828–835, 1996.

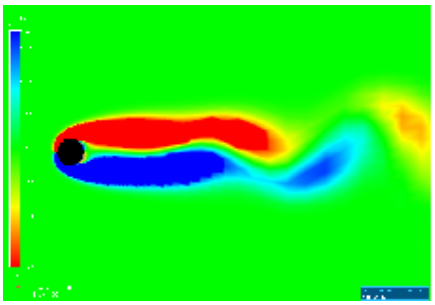

Fig. 13. Vorticity map at $t = 20s$.

[3] P. Huerre and P. Monkewitz, "Local and global instabilities in spatially developing flows," *Annu. Rev. Fluid Mech.*, vol. 22, pp. 473–537, 1990.

[4] K. Roussopoulos and P. Monkewitz, "Nonlinear modelling of vortex shedding control in cylinder wakes," *Physica D*, vol. 97, pp. 264–273, 1996.

[5] E. Lauga and T. Bewley, "H infinity control of linear global instability in models of non-parallel wakes," *Proceedings of the Second International Symposium on Turbulence and Shear Flow Phenomena*, vol. Stockholm, Sweden, 2001.

[6] E. Lauga and T. Bewley, "Performance of a linear robust control strategy on a nonlinear model of spatially-developing flows," *J. Fluid Mech*, vol. 512, pp. 343–374, 2004.

[7] O. M. Aamo and M. Krstic, "Global stabilization of a nonlinear ginzburg-landau model of vortex shedding," *Eur. J. Control*, vol. 10, no. 2, 2004.

[8] O. M. Aamo, A. Smyshlyaev, and M. Krstic, "Boundary control of the linearized ginzburg-landau model of vortex shedding," *SIAM J. Control Optim*, vol. 43, no. 6, pp. 1953–1971, 2005.

[9] O. M. Aamo, A. Smyshlyaev, M. Krstic, and B. Foss, "Output feedback boundary control of a ginzburg-landau model of vortex shedding," *IEEE Transactions on Automatic Control*, vol. 52, no. 4, pp. 742–748, 2007.

[10] P. Monkewitz, *private communication*.

[11] A. Smyshlyaev and M. Krstic, "Closed form boundary state feedbacks for a class of 1d partial integro-differential equations," *IEEE Transactions on Automatic Control*, vol. 49, pp. 2185–2202, 2004.

[12] W. J. Liu, "Boundary feedback stabilizaton of an unstable heat equation," *SIAM J. Control Optim*, vol. 42, pp. 1033–1043, 2003.

[13] M. Krstic and A. Smyshlyaev, *Boundary Control of PDEs: A Course on Backstepping Designs*. SIAM, 2008.

[14] M. Krstic, I. Kanellakopoulos, and P. Kokotovic, *Nonlinear and Adaptive Control Design*. Wiley, 1995.

[15] P. Catalano, M. Wang, G. Iaccarino, I. F. Sbalzarini, and P. Koumoutsakos, "Optimization of cylinder flow control via zero net mass flux actuators," in *Proceedings of the CTR summer program*, Center for Turbulence Research, Stanford University, 2002.

[16] P. Hoeijmakers, "Implementation of an extremum seeking controller for vortex shedding attenuation in a 2d cfd code." TU Eindhoven, 2008.